



Role of pH and Sintering Temperature on the Properties of Tetragonal–Cubic Phases Composed Copper Ferrite Nanoparticles

Akshay B. Ghumare¹ · Maheshkumar L. Mane¹ · Sagar E. Shirsath² · K. S. Lohar³

Received: 14 May 2018 / Accepted: 16 July 2018
© Springer Science+Business Media, LLC, part of Springer Nature 2018

Abstract

In the present investigation we have studied the role of varying pH and sintering temperature on the properties of copper ferrite nanoparticles synthesized from metal nitrate solutions by sol–gel auto-combustion technique. The CuFe_2O_4 samples were synthesized with varying pH values (without maintaining pH, pH 4 and 8). The careful analysis of X-ray diffraction (XRD) result showed that the pH provides boost to develop copper ferrite nanoparticles. The samples without maintaining pH suggested the presence of three different phases. The samples with pH values 4 and 8 showed the tetragonal structure. Crystal structure phase transformation of copper ferrite (pH 8) nanoparticles was studied under different sintering conditions. The prepared samples were characterized by XRD, field emission scanning electron microscopy, FTIR and magnetization. These copper ferrite nanoparticles sintered at different temperatures show combinations of cubic and tetragonal phases. The thermal behavior of as-prepared samples was confirmed by thermo gravimetric/differential thermal analyzer analysis. The morphology of materials was understood by SEM technique. The room temperature magnetic measurement proves strong redistribution of Cu^{2+} ions. Sintering temperature alerts the saturation magnetization (M_s) to a large extent from 9.26 to 25.15 emu/g.

Keywords Phase transformation · Sintering · Magnetic materials · Nanoparticles

1 Introduction

The spinel ferrites form an important class of magnetic materials having large scope in variety of technological and medical applications. Among the spinel ferrite copper ferrite nanoparticles have tremendous scope in the fundamental and applied research area. Recently, much attention has been paid on the copper oxide nanoparticles because they have wide range of applications such as magnetic storage media, gas sensors, semiconductors, batteries, solar energy transformation, heterogeneous catalysis and field emission [1–7]. Nanoparticles are much more active than larger particles because of their higher surface area, and they display unique

physical and chemical properties [8]. Presently, many efforts have been directed towards the synthesis of nanocrystalline CuFe_2O_4 to tailor its performance and attracted attention not only in the scientific field but also in industry application because when it treated under different conditions exhibits phase transition, modified semiconducting properties, shows electrical switching and tetragonality variation [9, 10].

Copper ferrite is important spinel ferrite which exists in tetragonal as well as cubic structures [11, 12]. The cubic phase is stable at low temperature and transforms to tetragonal phase with increasing sintering temperature due to Jahn–Teller distortion [13–15]. Tetragonal CuFe_2O_4 has inverse spinel structure with almost all Cu^{2+} ions occupying octahedral site, whereas Fe^{3+} ions shares both tetrahedral A and octahedral B-sites [16]. Spinel ferrite has been extensively studied due to its interesting properties with bottom up synthesis approach methods such as co-precipitation technique [17], solid state method [18], ball milling [19], reverse micelle [20], sol–gel [21, 22]. Among these physical and chemical methods, a sol–gel auto-combustion method has advantages of low temperature synthesis, economical, good control over stoichiometry and crystallite size. Recently many research scientists

✉ Maheshkumar L. Mane
mane.maheshkumar@hotmail.com

¹ Shikshan Maharshi Guruvarya R. G. Shinde Mahavidyalaya, Paranda Dist., Osmanabad, MS, India

² Department of Physics, Vivekanand College, Aurangabad, MS 431004, India

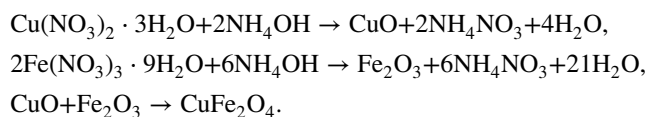
³ Shrikrishana Mahavidyalaya, Gunjoti Dist., Osmanabad, MS, India

investigated the influence of pH on tailoring the magnetic properties of different ferrite nanoparticles [23–25]. On the hand, to the best of our knowledge no systematic investigations are available, which reveals the influence of nature of synthetic condition on nano-sized copper ferrite material synthesized by sol–gel auto-combustion method.

In the present study, we report the phase formation/transformation of copper ferrite nanoparticles synthesized by sol–gel auto-combustion technique. We successfully obtained tetragonal phase of copper ferrite at low sintering temperature. The yields and product purity were remarkable. We expect this method to find economical and relatively efficient as compared to conventional methods for extensive application in the field of industrial chemistry, gas sensors and catalysis.

2 Experimental Technique

Nanocrystalline copper ferrite was synthesized by using the citrate–nitrate sol–gel auto-combustion technique. Analytical grade $\text{Cu}(\text{NO}_3)_2 \cdot 3\text{H}_2\text{O}$, $\text{Fe}(\text{NO}_3)_3 \cdot 9\text{H}_2\text{O}$ and $\text{C}_6\text{H}_8\text{O}_7$ were dissolved in distilled water in their respective stoichiometry to obtain a homogeneous solution. The metal nitrate to citric acid molar ratio was 1:3. The citric acid acts as a fuel that initiates the combustion process but does not take part in the formation of copper ferrite. Initially the material was prepared without addition of ammonia (without maintaining pH), further the materials were prepared at pH 4 (acidic) and 8 (basic) by adding drop-wise ammonia. The control of pH during chemical synthesis plays crucial role in tailoring the properties of ferrite material. The above mixture was continuously stirred using a magnetic stirrer with hot plate keeping the temperature at 70 °C in order to remove excess water until the viscous brown gel formation. The gel so formed continuously stirred at 80 °C to form sol and finally sol was continuously heated at 120 °C to initiate self-combustion process. The final product was ground to form a fine powder. The loose powder was sintered at 600 °C for 6 h after confirmation by thermo gravimetric/differential thermal analyzer (TG/DTA) analysis. The produced fine powder at pH 8 was sintered at varying temperatures 600, 800 and 1000 °C. The mechanism involved in the formation of copper ferrite nanoparticles by sol–gel auto-combustion technique can be represented as,



The thermal behavior of as-prepared samples was confirmed by TG/DTA (Make: Perkin Elmer model, Model: diamond TG/DTA). The as-prepared and sintered copper ferrite nanoparticles were characterized by powder X-ray diffraction (XRD) technique (Philips) with θ – 2θ geometry

using $\text{Cu K}\alpha$ radiations ($\lambda = 1.5406 \text{ \AA}$) to identify crystal phase of samples. The surface morphology and chemical composition (EDS) of samples was investigated by scanning electron microscopy (FEG-SEM model JSM-7600F). In addition, Fourier transformation infrared spectroscopy was carried out in a KBr medium at wave numbers ranging from 400 to 4000 cm^{-1} . The magnetic measurements were carried out at room temperature using pulse field hysteresis loop technique.

3 Results and Discussion

Figure 1 represents the thermo-chemical behavior of as-prepared copper ferrite nanoparticles in the temperature range of ambient to 825 °C with heating rate of 5 °C/min were examined by TG/DTA. In the heat treatment of ferrite various processes like dehydration and decomposition of residual nitrate takes place. TGA curve represents different regions of weight loss, which are further confirmed by the occurrence of peaks on the DTA curve. The TGA analysis shows weight loss is about 1.167% at 317.60 °C which is due to dehydroxylation of ferrite powder. In DTA only one endothermic peak is observed at around 200–400 °C which is due to evaporation of water and decomposition of organic compounds and nitrates. No additional weight loss was observed at temperatures above the decomposition temperature (500 °C), which reveals the formation of copper ferrite nanoparticles.

The compositional stoichiometry of the CuFe_2O_4 (pH 8) was investigated using EDS image analysis on various regions of the prepared samples, is shown in Fig. 2. Composition determined by EDS is compared to the relative amount of metal cations ions used to make the particles of copper ferrite nanoparticles. The percentage of iron is always found to be quite constant. Hence, the composition of Cu, Fe and

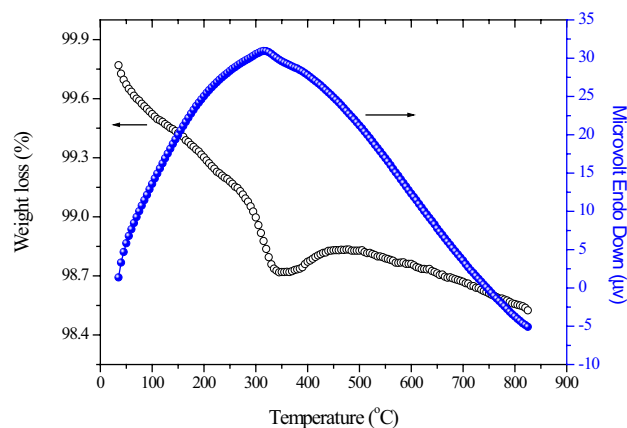


Fig. 1 TG/DTA for as-prepared CuFe_2O_4

O elements is similar to the composition of the mixture used for the synthesis.

The powder XRD patterns recorded at room temperature in the 2θ range of 20° – 80° for copper ferrite nanoparticles with varying pH is depicted in Fig. 3. The sample prepared with pH 8 confirmed the tetragonal crystal structure by comparing XRD results with standard data (JCPDS 34-0425). From the XRD patterns, it was observed that the samples without maintaining the pH exhibits the phases of CuO, α - Fe_2O_3 and ν - Fe_2O_3 . The sample with pH 4 show tetragonal structure with extra peaks of α - Fe_2O_3 and ν - Fe_2O_3 phase. The diffraction peaks changes in both intensity and Bragg's angle (2θ) with pH as a result of the change in crystal structure parameters. The pH of solution plays a crucial role in deciding the final composition of product. When the pH of solution is maintained at 8 the Fe_2O_3 phase gets disappeared also the peak intensity increases and peaks becomes sharper which indicates effect of pH on the degree of crystallinity [26, 27]. Shirsath et al. [28] reported that when the pH of solution is in alkaline state the citric acid completely chelate the metal cations which cause the uniform distribution of cations in the solid precursor.

The Bragg's law is employed on XRD data to determine interplaner distance d_{hkl} , which is used to estimate the lattice parameter for most prominent peak. The lattice constant 'a' decreases whereas 'c' increases resulting increase in c/a ratio. The value of c/a is > 1 for the pH 4 and 8 showing tetragonal Jahn–Teller distortion. The average crystallite size of each sample was calculated by Scherrer's formula [29]. The crystallite size reveals the increasing trend with increasing pH (Fig. 4).

FTIR spectra recorded in Fig. 5 shows effect of pH on the formation of copper ferrite nanoparticles. The spectrum reflects two absorption bands appearing around 600 and 400 cm^{-1} , respectively are assigned to metal–oxygen

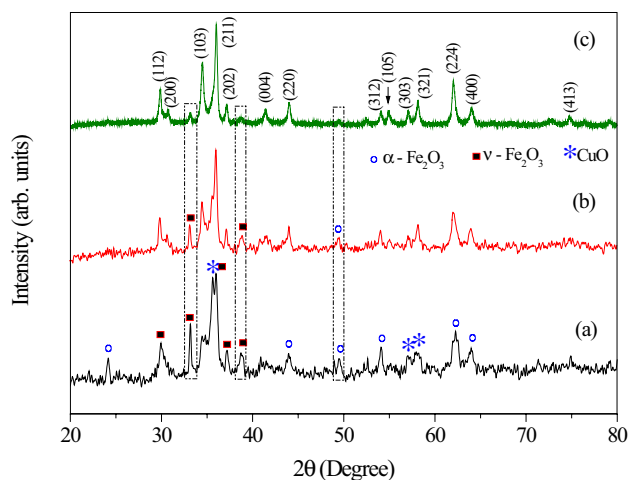


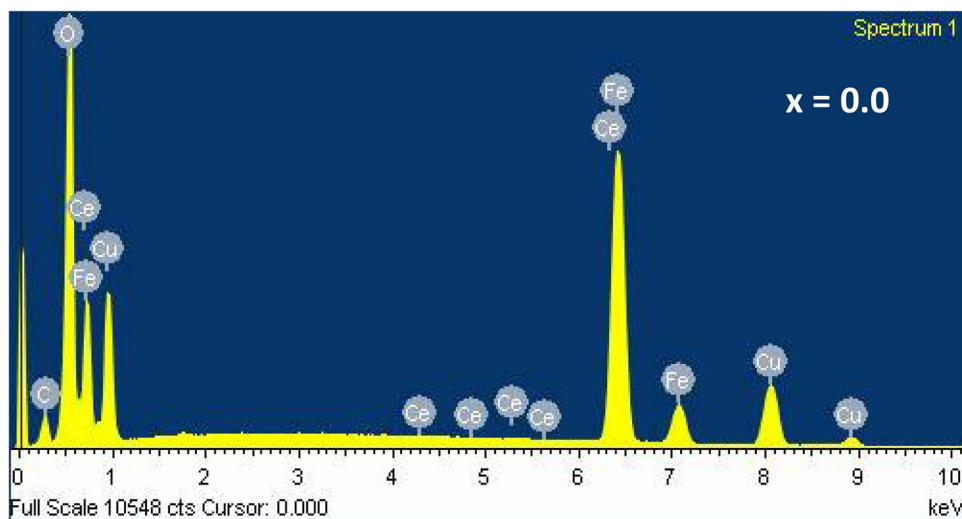
Fig. 3 X-ray diffraction patterns for CuFe_2O_4 (a) without maintaining pH, (b) pH 4, and (c) pH 8

stretching. It has been noticed that peak intensities decreases and peak shifts to higher values with increase in pH.

The morphology of the synthesized samples was investigated using field emission SEM (FESEM) at different pH values. Figure 6 reveals significant influence of pH on particles size of synthesized materials. The release of large amount of gases during the synthesis combustion process leads to formation of pores and voids in the material. The variation in particle size is negligible for samples prepared in the acidic condition (without addition of ammonia and pH 4) whereas the variation in particle size is significant when the samples prepared in the alkaline condition (pH 8).

Effect of pH variation on the magnetic property of nanocrystalline copper ferrite is shown in Fig. 7. The saturation magnetization shows pH plays crucial role as a chelating agent during the synthesis process of magnetic materials.

Fig. 2 EDS analysis for CuFe_2O_4 nanoparticles



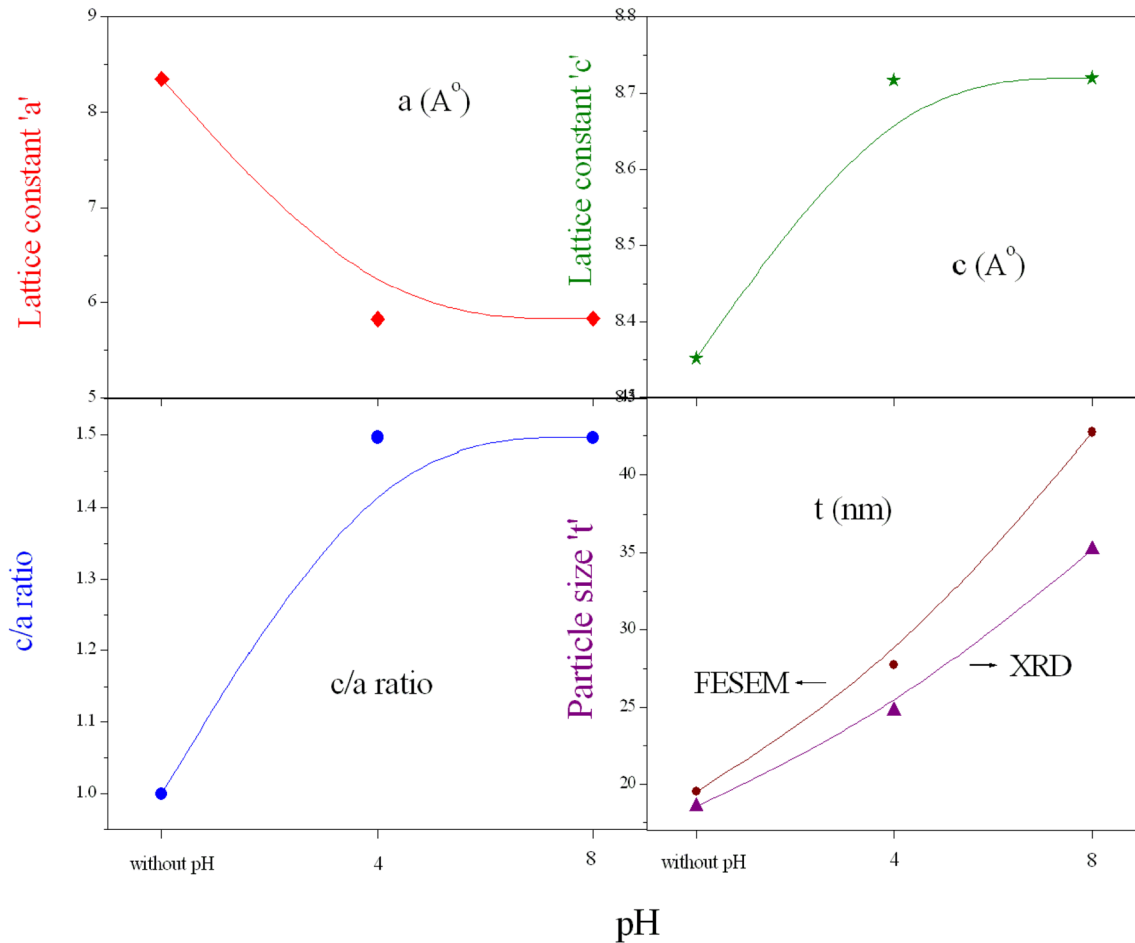


Fig. 4 Variation of lattice parameter, c/a ratio and particle size for different pH values

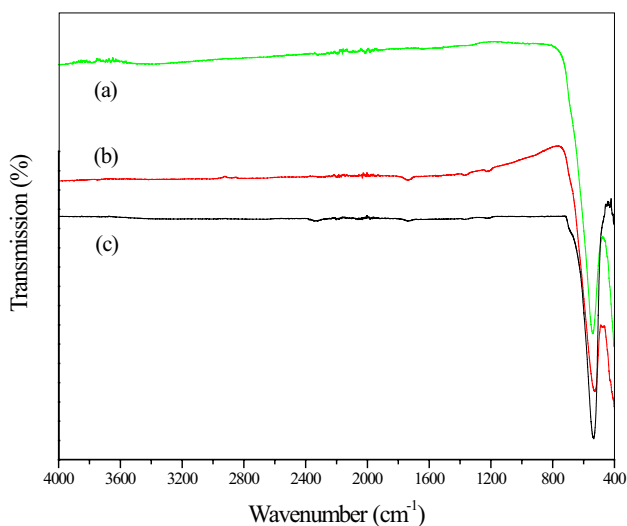


Fig. 5 FTIR spectra for CuFe_2O_4 (a) without maintaining pH, (b) pH 4 and (c) pH 8

The saturation magnetization increases with increase in pH value due to change in particle size and morphology of copper ferrite.

Powder XRD patterns of product sintered at different temperatures (Fig. 8) indicate that the material is mainly composed of CuFe_2O_4 . The 2θ Bragg positions and peak intensities of all reflections confirms well with standard XRD pattern of CuFe_2O_4 (JCPDS 34-0425 and 77-0010). The as-prepared XRD pattern indicates the characteristics of cubic copper ferrite ($c\text{-CuFe}_2\text{O}_4$), the copper ferrite powder sintered at 600 and 800 °C indicates the characteristics of tetragonal structure ($t\text{-CuFe}_2\text{O}_4$). This structure phase transformation of CuFe_2O_4 from cubic–tetragonal–cubic can be assigned to the tetragonal distortion of Jahn–Teller effect of Cu^{2+} ions (d^9). When odd number of electrons are present in the e_g orbitals Jahn–Teller effect is more common in octahedral complexes. In CuFe_2O_4 the Cu^{2+} ions exhibit d^9 configuration where three electrons are present in the e_g orbitals. Therefore Jahn–Teller distortion becomes more pronounced in copper ferrites. In spinel ferrite Cu^{2+} ions occupy both tetrahedral as well as octahedral sites at room

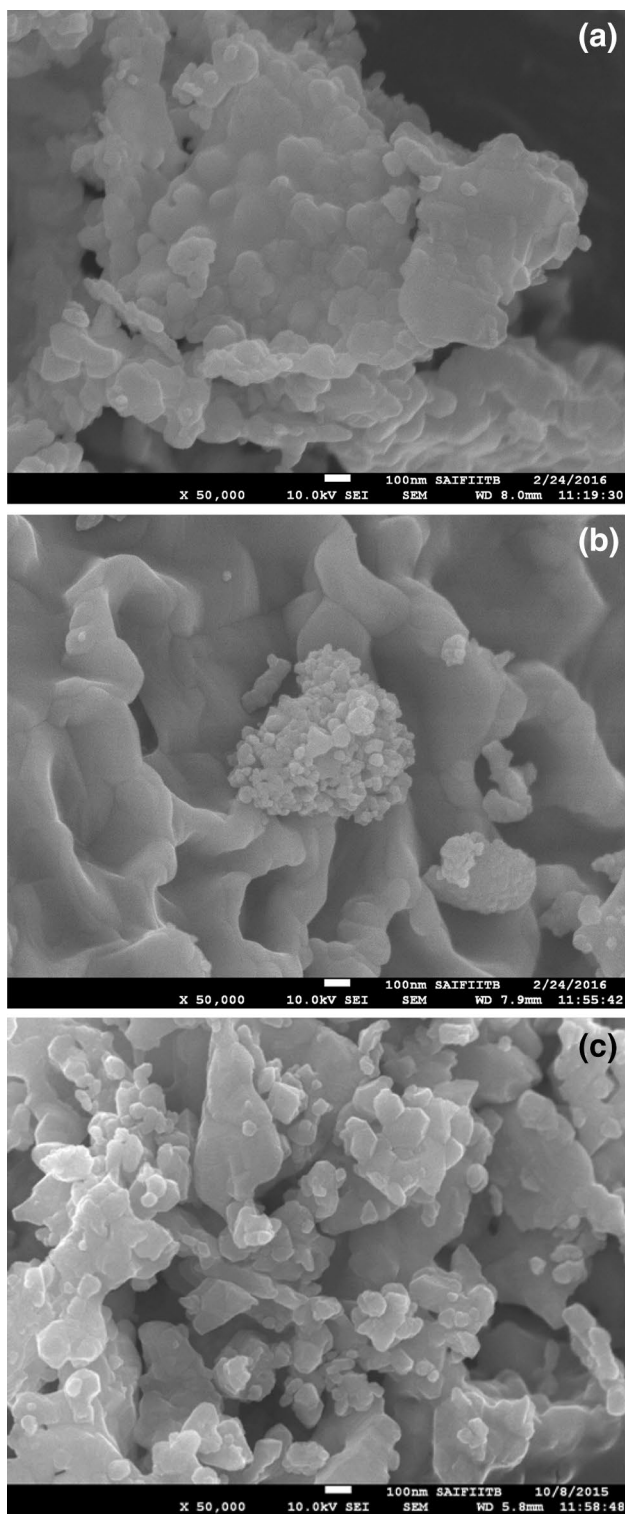


Fig. 6 FESEM images **a** without maintaining pH, **b** pH 4, and **c** pH 8

temperature with cubic crystal structure, as temperature increases the Cu^{2+} ions migrates from tetrahedral to octahedral sites which causes distortion in lattice. The sample sintered at $600\text{ }^\circ\text{C}$ shows Jahn–Teller distortion containing

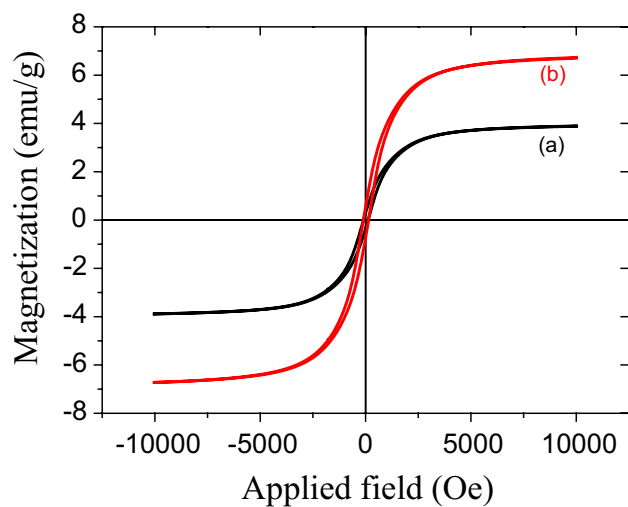


Fig. 7 Magnetization curves for CuFe_2O_4 **(a)** without maintaining pH and **(b)** pH 4

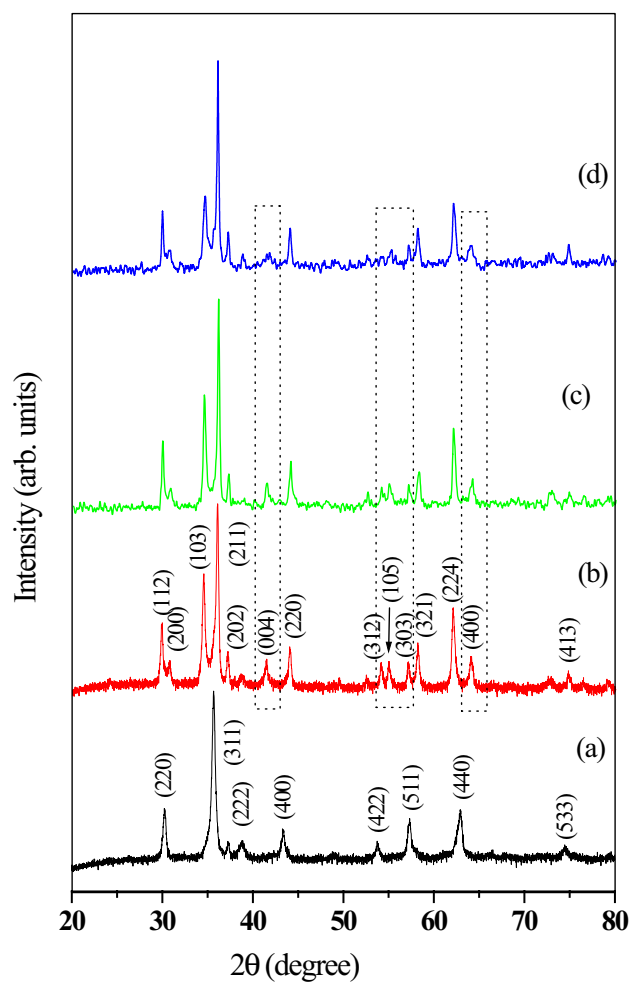
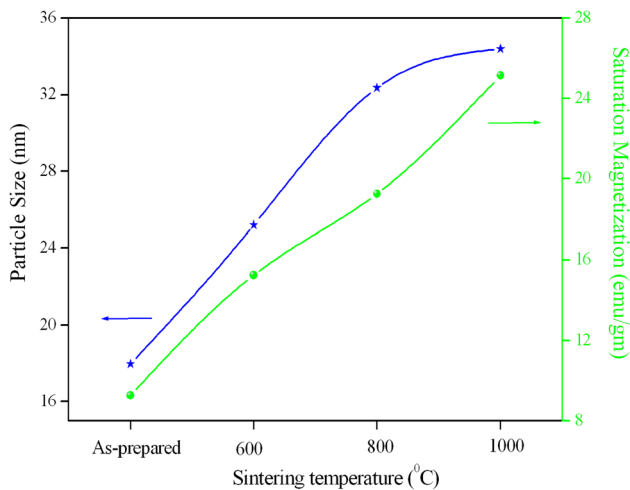


Fig. 8 X-ray diffraction patterns for CuFe_2O_4 **(a)** as-prepared, **(b)** $600\text{ }^\circ\text{C}$, **(c)** $800\text{ }^\circ\text{C}$ and **(d)** $1000\text{ }^\circ\text{C}$

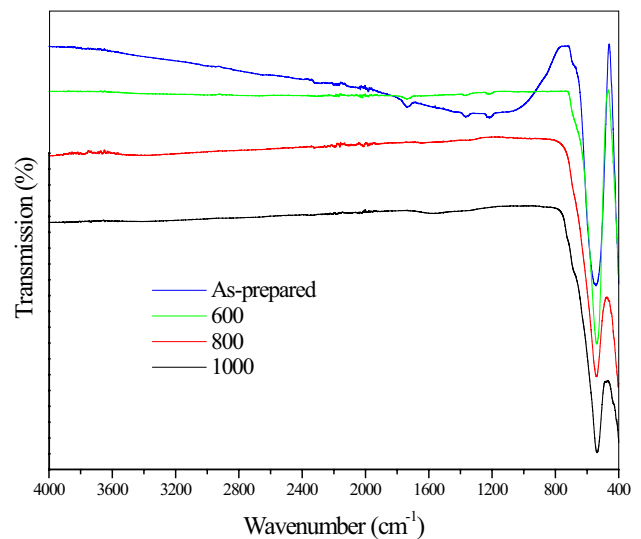
Table 1 Lattice constant (a, c), c/a ratio, particle size, saturation magnetization (M_s), observed magnetic moment ($n_{\text{B}}^{\text{obs}}$)

	Lattice constants		c/a	Particle size (nm)		M_s (emu/g)	$n_{\text{B}}^{\text{obs}}$
	a	c		XRD	SEM		
As-prepared	8.346	8.346	1.0000	17.97	–	9.26	0.3967
600	5.830	8.720	1.4957	25.20	44.5	15.25	0.6532
800	5.800	8.710	1.5017	32.36	51.9	19.26	0.8250
1000	5.815	8.745	1.5038	34.39	54.3	25.15	1.0773

**Fig. 9** Variation of particle size and saturation magnetization with sintering temperature

sufficient concentration of Cu^{2+} ions at octahedral sites resulting in tetragonal structure ($c/a > 1$) [30, 31]. The values of c/a increases with sintering temperature and are given in Table 1. Amer et al. [12] reported that the tetragonal Jahn–Teller distortion of Cu^{2+} ions can be achieved at 900 °C. In present investigation the distortion of Cu^{2+} ions was observed relatively at low temperature at 600 °C. The copper ferrite powder sintered at 1000 °C shows mixture of cubic and tetragonal crystal phase. The sample sintered at high temperature retains the phase with cubic crystal structure. The peak intensities corresponding to Bragg angles 34.34, 41.26, 54.06, 54.93, 57.07 and 64.20 decreases and increases at 38.64 for the sample sintered at 1000 °C. The diffraction peak becomes sharper and intense, because of increase in crystallinity and crystal size. The particle size of order of 17–34 nm (Fig. 9), calculated from broadening of most intense peak using Scherrer formula. The values of structural parameters such as lattice constant and particle size are given in Table 1.

The FTIR spectra recorded in the range of 400–4000 cm^{-1} is depicted in Fig. 10, provides useful information about nature and structure of copper ferrite nanoparticles. The spectra of all samples reveal the presence of two metal–oxygen absorption band in the range of 400–600 cm^{-1} [32]. In the FTIR spectrum (Fig. 7) absorption band observed in the

**Fig. 10** FTIR spectra for CuFe_2O_4 (a) as-prepared, (b) 600 °C, (c) 800 °C and (d) 1000 °C

range of 530–550 cm^{-1} was assigned to intrinsic stretching vibrations of the metals at the tetrahedral site (A), and the band observed at 400 cm^{-1} , is assigned to octahedral (B) metal stretching [33] which confirms the formation of spinel ferrite material. The as-prepared sample shows the characteristic peaks at 1736, 1371 and 1216 cm^{-1} corresponds to O–H bending vibrations and N–O stretching vibrations which indicates the incomplete formation of sample [17, 34]. These vibrations gets disappear in the FTIR spectrum of sintered samples which reveals the complete formation of spinel copper ferrite nanoparticles.

The microstructure of the samples sintered at 800 and 1000 °C is further investigated by FESEM analysis, shown in Fig. 11a, b, respectively, indicates the presence of single phase. The sintered samples exhibit a grain growth with an average grain size ~ 51 –55 nm.

The magnetic properties of copper ferrite nanoparticles were measured by using pulse field hysteresis loop tracer at room temperature. The magnetic behavior of copper ferrite samples has strongly influenced by sintering temperature. Figure 12 indicates the typical magnetization curves. It can be observed from magnetization loops that the saturation magnetization (M_s) values increases with increasing the

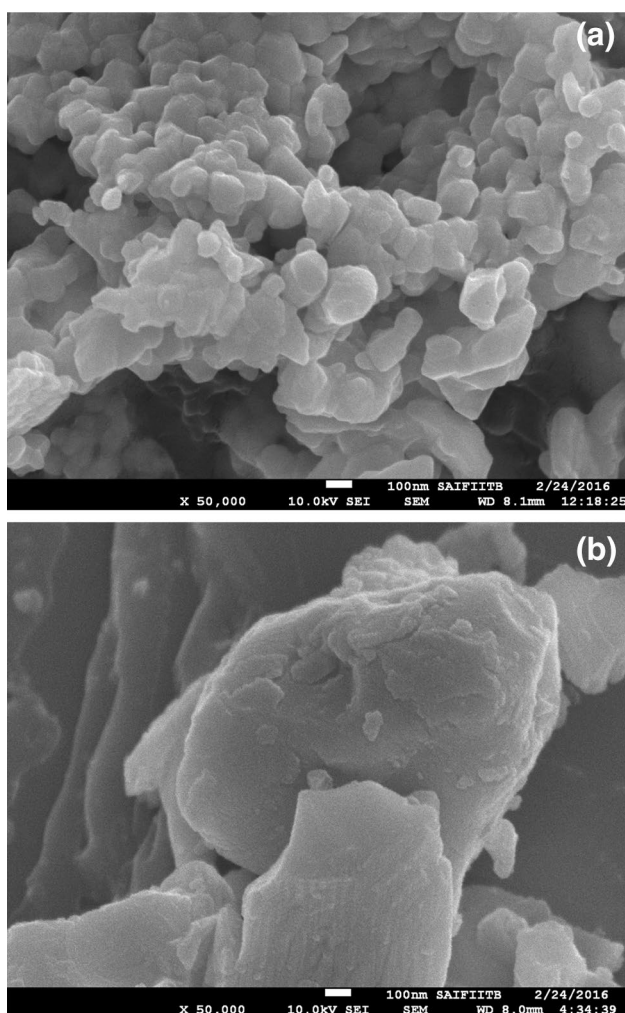


Fig. 11 FESEM images for CuFe_2O_4 **a** 800 °C and **b** 1000 °C

sintering temperature as a result of the gradual increase in the crystallinity and particle size confirmed from XRD and SEM analysis (Fig. 9). The observed magnetic moment was calculated by using the formula [35] $n_B^{\text{obs}} = \frac{MW \times M_s}{5585}$ where MW is molecular weight of the compound and M_s is saturation magnetization. The observed magnetic moment increases with increase in sintering temperature (Table 1).

4 Conclusions

The presented result reveals the importance of pH as chelating agent in the formation of ferrite nanoparticles. We also successfully studied the role sintering temperature on phase transformation of copper ferrite nanoparticles synthesized by sol-gel auto-combustion technique. The samples with pH values 4 and 8 showed the tetragonal structure. The lattice constant 'a' decreases, whereas 'c' and c/a ratio improved due to increase in alkaline nature of samples. The FESEM

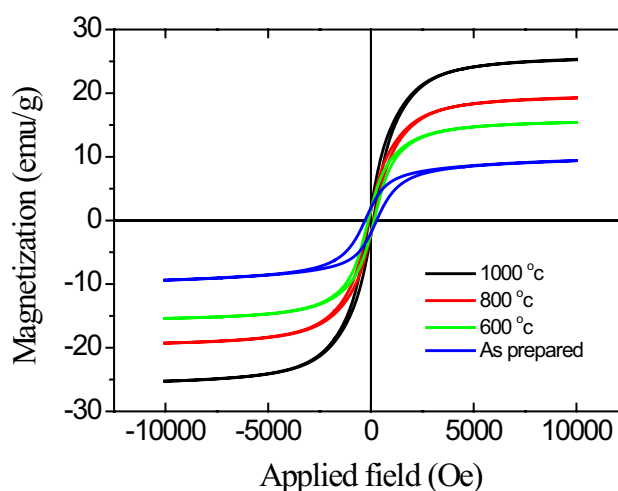


Fig. 12 Magnetization curves for CuFe_2O_4 nanoparticles

analysis further proved the influence of pH value on morphological behavior. Results showed that increasing pH value contributed to increase in particle size. The structural investigations of samples (pH 8) proved that as-prepared material consist of cubic phase whereas tetragonal phase was observed at relatively low temperature (600 °C) due to tetragonal Jahn–Teller distortion. Increasing temperature treatment up to 1000 °C led to formation of an intermediate phase of cubic and tetragonal orientation. FTIR study reveals two main absorption bands in the range of 600–400 cm^{-1} . The FESEM and XRD analysis indicates the growth of particles with sintering temperature increases. The magnetic properties are strongly influenced by sintering temperature. We expect this sol-gel auto-combustion method finds economical importance, low cost and relatively better efficiency as compared to conventional methods.

Acknowledgements ABG gratefully acknowledges SAIF, IIT Bombay for granting access to TG/DTA, FESEM and EDS research facilities.

References

1. W. Ponhan, S. Maensiri, Fabrication and magnetic properties of electrospun copper ferrite (CuFe_2O_4) nanofibers. *Solid State Sci.* **11**, 479–484 (2009)
2. R. Köferstein, T. Walther, D. Hesse, S.G. Ebbinghaus, Crystal-lite-growth, phase transition, magnetic properties, and sintering behaviour of nano- CuFe_2O_4 powders prepared by a combustion-like process. *J. Solid State Chem.* **213**, 57–64 (2014)
3. M.A. Haija, A.F.S. Abu-Hani, N. Hamdan, S. Stephen, A.I. Ayesh, Characterization of H_2S gas sensor based on CuFe_2O_4 nanoparticles. *J. Alloys Compds* **690**, 461–468 (2017)
4. S. Sonia, S. Poongodi, P.S. Kumar, D. Mangalaraj, N. Ponpandian, C. Viswanathan, Hydrothermal synthesis of highly stable CuO nanostructures for efficient photo catalytic degradation of organic dyes. *Mater. Sci. Semicond. Process.* **30**, 585–591 (2015)

5. A. Suresh Kumar, B. Thulasiram, S. Bala Laxmi, V.S. Rawat, B. Sreedhar, Magnetic CuFe_2O_4 nanoparticles: a retrievable catalyst for oxidative amidation of aldehydes with amine hydrochloride salts. *Tetrahedron* **70**, 6059–6067 (2014)
6. M. Sabbaghan, A.S. Shahvelayati, K. Madankar, CuO nanostructures: optical properties and morphology control by pyridinium-based ionic liquids. *Spectrochim. Acta A* **135**, 662–668 (2015)
7. S. Park, S. Kim, S. Park, C. Lee, Facile synthesis of CuO nanotubes and their formation mechanism. *Mater. Lett.* **138**, 110–112 (2015)
8. C.Y. Chen, C.L. Chiang, Preparation of cotton with antibacterial silver nanoparticles. *Mater. Lett.* **62**, 3607–3609 (2008)
9. G. Saito, S. Hosokai, M. Tsubota, T. Akiyama, Synthesis of copper/copper oxide nanoparticles by solution plasma. *J. Appl. Phys.* **110**, 023302 (2011)
10. M.M. Rashad, R.M. Mohamed, M.A. Ibrahim, L.F.M. Ismail, E.A. Abdel-Aal, Magnetic and catalytic properties of cubic copper ferrite nanopowders synthesized from secondary resources. *Adv. Powder Technol.* **23**, 315–323 (2012)
11. S. Tao, F. Gao, X. Liu, O.T. Sørensen, Preparation and gas-sensing properties of CuFe_2O_4 at reduced temperature. *Mater. Sci. Eng. B* **77**, 172–176 (2000)
12. M.A. Amer, T. Meaz, A. Hashhash, S. Attalah, F. Fakhry, Structural phase transformations of as-synthesized Cu -nanoferrites by annealing process. *J. Alloys Compds* **649**, 712–720 (2015)
13. M.H. Abdellatif, C. Innocenti, I. Liakos, A. Scarpellini, S. Marras, M. Salerno, Effect of Jahn–Teller distortion on the short range magnetic order in copper ferrite. *J. Magn. Magn. Mater.* **424**, 402–409 (2017)
14. S. Kimura, T. Mashino, T. Hiroki, D. Shigeoka, N. Sakai, L. Zhu, Y. Ichiyangi, Effect of heat treatment on Jahn–Teller distortion and magnetization in Cu ferrite nanoparticles. *Thermochim. Acta* **532**, 119–122 (2012)
15. I. Nedkov, R.E. Vandenberghe, T. Marinova, P. Tailhades, T. Merodiiska, I. Avramova, Magnetic structure and collective Jahn–Teller distortions in nanostructured particles of CuFe_2O_4 . *Appl. Surf. Sci.* **253**(5), 2589–2596 (2006)
16. Z. Xing, et al., One-step solid state reaction to selectively fabricate cubic and tetragonal CuFe_2O_4 anode material for high power lithium ion batteries. *Electrochim. Acta* **102**, 51–57 (2013)
17. M.A. Malana, R.B. Qureshi, M.N. Ashiq, Z.I. Zafar, Synthesis, electrical and dielectric characterization of cerium doped nano copper ferrites. *Mater. Res. Bull.* **48**, 4775–4779 (2013)
18. M.L. Mane, R. Sundar, K. Ranganathan, S.M. Oak, K.M. Jadhav, Effects of Nd:YAG laser irradiation on structural and magnetic properties of $\text{Li}_{0.5}\text{Fe}_{2.5}\text{O}_4$. *Nucl. Instrum. Methods B* **269**, 466–471 (2011)
19. J. Chen, Y. Wang, Y. Deng, Highly ordered CoFe_2O_4 nanowires array prepared via a modified sol–gel templated approach and its optical and magnetic properties. *J. Alloy Compds* **552**, 65–69 (2013)
20. M. Hashim, S.E. Shirsath, S.S. Meena, M.L. Mane, S. Kumar, P. Bhatt, R. Kumar, N.K. Prasad, S.K. Alla, J. Shah, R.K. Kotnala, K.A. Mohammedi, E. Senturk, Alimuddin, Manganese ferrite prepared using reverse micelle process: structural and magnetic properties characterization. *J. Alloy. Compds* **642**, 70–77 (2015)
21. S.S. Shirsath, S.S. Jadhav, M.L. Mane, S. Li, in *Handbook of Sol–Gel Science and Technology* (Springer, Berlin, 2017), pp. 1–41
22. G. Raja, S. Gopinath, R. Azhagu Raj, A.K. Shukla, M.S. Alhoshan, K. Sivakumar, Comparative investigation of CuFe_2O_4 nano and microstructures for structural, morphological, optical and magnetic properties. *Physica E* **83**, 69–73 (2016)
23. P. Iranmanesh, S. Saeednia, M. Mehran, S. Rashidi Dafeh, Modified structural and magnetic properties of nanocrystalline MnFe_2O_4 by pH in capping agent free co-precipitation method. *J. Magn. Magn. Mater.* **425**, 31–36 (2017)
24. J. de Vicente, A.V. Delgado, R.C. Plaza, J.D.G. Durán, F. González-Caballero, Stability of cobalt ferrite colloidal particles. Effect of pH and applied magnetic fields. *Langmuir* **16**, 7954–7961 (2000)
25. S.A. Seyyed Ebrahimi, S.M. Masoudpanah, Effects of pH and citric acid content on the structure and magnetic properties of MnZn ferrite nanoparticles synthesized by sol–gel autocombustion method. *J. Magn. Magn. Mater.* **357**, 77–81 (2014)
26. X. Huang, J. Zhang, W. Wang, T. Sang, B. Song, H. Zhu, W. Rao, C. Wong, Effect of pH value on electromagnetic loss properties of Co–Zn ferrite prepared via coprecipitation method. *J. Magn. Magn. Mater.* **405**, 36–41 (2016)
27. N. Lwin, R. Othman, A.F.M. Noor, S. Sreekantan, T.C. Yong, R. Singh, C.-C. Tin, Influence of pH on the physical and electromagnetic properties of Mg–Mn ferrite synthesized by a solution combustion method. *Mater. Charact.* **110**, 109–115 (2015)
28. S.E. Shirsath, M.L. Mane, Y. Yasukawa, X. Liu, A. Morisako, Chemical tuning of structure formation and combustion process in $\text{CoDy}_{0.1}\text{Fe}_{1.9}\text{O}_4$ nanoparticles: influence@pH. *J. Nanopart. Res.* **15**, 1976 (2013)
29. B.D. Cullity, *Elements of X-Ray Diffraction*, 2nd edn. (Addison-Wesley, Reading, 1978)
30. C. Baubet, Ph. Tailhades, C. Bonningue, A. Rousset, Z. Simsa, Influence of tetragonal distortion on magnetic and magneto-optical properties of copper ferrite films. *J. Phys. Chem. Solids* **61**, 863–867 (2000)
31. J.B. Goodenough, Jahn–Teller phenomena in solids. *Annu. Rev. Mater. Sci.* **28**, 1–27 (1998)
32. B.G. Toksha, S.E. Shirsath, M.L. Mane, S.M. Patange, S.S. Jadhav, K.M. Jadhav, Autocombustion high-temperature synthesis, structural, and magnetic properties of $\text{CoCr}_x\text{Fe}_{2-x}\text{O}_4$ ($0 \leq x \leq 1.0$). *J. Phys. Chem. C* **115**, 20905–20912 (2011)
33. J.L. Gunjekar, A.M. More, K.V. Gurav, C.D. Lokhande, Chemical synthesis of spinel nickel ferrite (NiFe_2O_4) nano-sheets. *Appl. Surf. Sci.* **254**, 5844–5848 (2008)
34. G.X. Cao, T. Liu, Q.H. Zhang, H.Z. Wang, Synthesis and characterization of nanometer copper ferrite by auto-combustion. *Adv. Mater. Res.* **347–353**, 3472–3476 (2012)
35. R.H. Kadam, A.R. Biradar, M.L. Mane, S.E. Shirsath, Sol–gel auto-combustion synthesis of $\text{Li}_{3x}\text{MnFe}_{2-x}\text{O}_4$ and their characterizations. *J. Appl. Phys.* **112**, 043902 (2012)